IEEE Access
Multidisciplinary | Rapid Review | Open Access Journal

Received October 24, 2019, accepted November 8, 2019, date of publication November 13, 2019, date of current version December 2, 2019.

Digital Object Identifier 10.1109/ACCESS.2019.2953311

Dual-Functional MIMO Antenna Array With High Isolation for 5G/WLAN Applications in Smartphones

HUANQING ZOU[1,2], YIXIN LI[3], BIN XU[4], YUANQING CHEN[1,2], (Student Member, IEEE), HAO JIN[1,2], GUANGLI YANG[1,2], (Member, IEEE), AND YONG LUO[1,2]

[1]Shanghai Institute for Advanced Communication and Data Science, Shanghai University, Shanghai 200444, China
[2]Key Laboratory of Specialty Fiber Optics and Optical Access Networks, Shanghai University, Shanghai 200444, China
[3]School of Electronic and Information Engineering, South China University of Technology, Guangzhou 510641, China
[4]Qualcomm, San Diego, CA 92122, USA

Corresponding author: Yong Luo (y_luo@foxmail.com)

This work was supported by the Shanghai "Eastern Scholarship."

ABSTRACT A dual-functional antenna array operating in the long term evolution (LTE) band 42 (3.4–3.6 GHz) and 5.8-GHz wireless wide area network (WLAN) band (5.725–5.875 GHz) for multiple-input multiple-output (MIMO) applications in 5G smartphones is proposed. The proposed 8-antenna array is composed of two different antenna elements, namely, the folded L-shaped antenna and couple-fed U-shaped antenna. It can be applied in the 8 × 8 (by using 8 antenna elements) and 4 × 4 (by using 4 antenna elements) MIMO system across the LTE band 42 and 5.8-GHz WLAN band, respectively. The quasi-orthogonal polarization, balanced mode excitation and pattern diversity are properly used to achieve high isolation within the operation bands. A prototype of the proposed antenna array was fabricated and measured. The measured isolations in the LTE band 42 (6-dB impedance matching) and 5.8-GHz WLAN band (10-dB impedance matching) are better than 17.1 dB and 34.6 dB, respectively. The total efficiencies are 45%–62% and 52%–59% in the two operation bands, respectively. Besides, the measured envelope correlation coefficients (ECCs) are less than 0.045 and 0.0001, the calculated peak ergodic channel capacities are 37.9 bps/Hz and 19.3 bps/Hz in the 8 × 8 or 4 × 4 MIMO system across the operation bands. Furthermore, user's hand and head effects are investigated and desirable results are obtained. The above results show that this proposed antenna array is a good candidate for MIMO applications in smartphones.

INDEX TERMS 5G communication, high-isolation, multi-input multi-output (MIMO), smartphone antenna.

I. INTRODUCTION

With the growing demands of higher data rates in the future 5G communication system, the multiple input multiple output (MIMO) technology has attracted increasing attention both in industry and academia [1]. However, it faces a great challenge to place multiple antennas in the limited design space while achieving high isolation and multi-band. In [2]–[6], some multi-band antenna arrays operating in the sub-6 GHz bands (5G frequency bands below 6 GHz) for future 5G smartphones have been proposed. However, the isolations of these multi-band antenna arrays are merely better than about 10 dB, because it is very challenging to reduce the mutual coupling of the high-order MIMO antenna array. Various types of decoupling techniques have been reported to achieve high isolation, such as the neutralization line [7] and parasitic structure [8]. The work in [9] has achieved high isolation by loading decoupling elements, but the decoupling elements sacrifice the total efficiency of antenna array. In addition, several high-isolation antenna arrays operating in the sub-6 GHz bands for smartphone application have also been reported in [10]–[18]. However, these works only support single band operation.

The future 5G communication network is a multi-network converged system. The convergence of licensed 5G long term evolution (LTE) bands and unlicensed wireless wide area network (WLAN) spectrum can well meet the growing traffic demand in the heterogeneous networks [19], [20]. Even though other works in [21]–[25] have obtained desirable results, these antenna arrays rarely support the WLAN

The associate editor coordinating the review of this manuscript and approving it for publication was Giorgio Montisci.

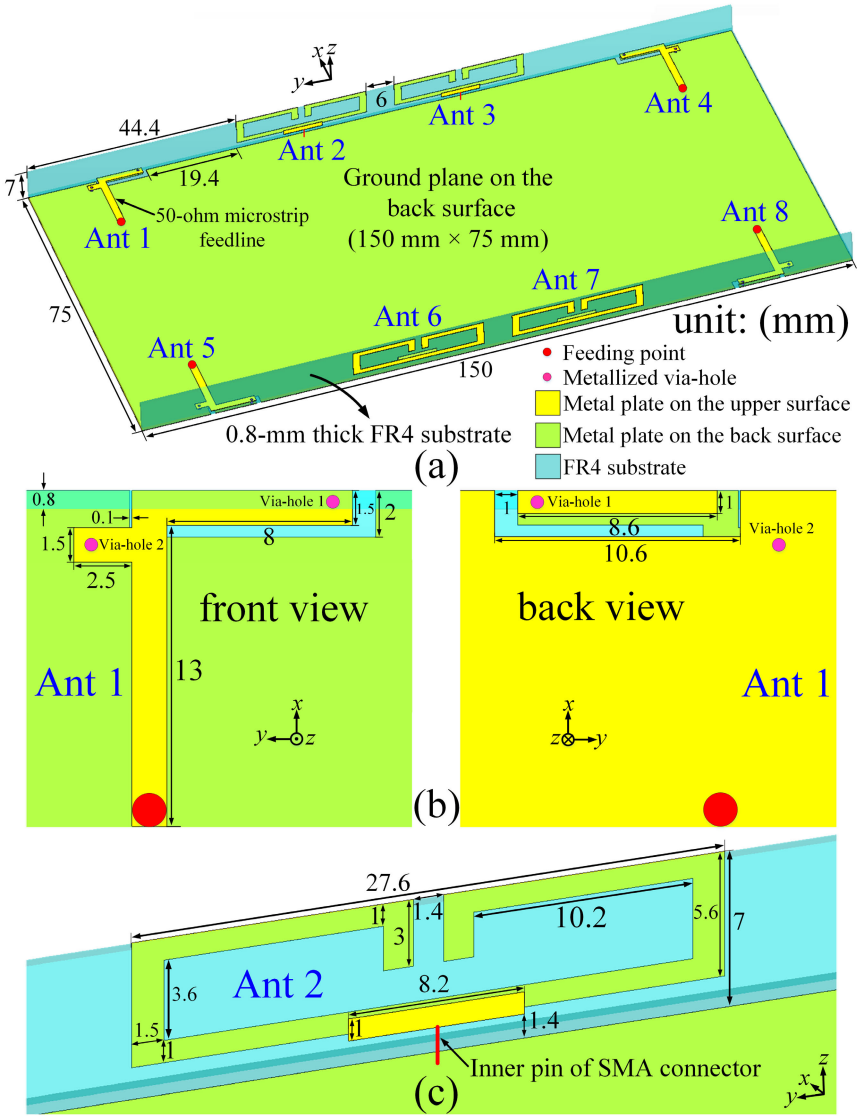

FIGURE 1. Geometry and detailed structure of the proposed MIMO antenna array: (a) overall view of the antenna array, (b) the folded L-shaped antenna (FLA), (c) the couple-fed U-shaped antenna (CUA).

bands, such as the 5.8-GHz WLAN band (5.725–5.875 GHz). Among the currently announced sub-6 GHz bands, the LTE band 42 (3.4–3.6 GHz) is the most widely adopted band for future 5G deployment. Presently, the design of high-isolation MIMO antenna array covering the LTE band 42 and WLAN band is rarely reported.

In the article, a dual-functional antenna array that covers both the LTE band 42 and 5.8-GHz WLAN band for 8 × 8 (by using 8 antenna elements) and 4 × 4 (by using 4 antenna elements) MIMO applications in smartphones is proposed. The proposed antenna array consists of two types of antenna elements, namely, the folded L-shaped antenna (FLA) and couple-fed U-shaped antenna (CUA). The FLAs support dual-band operation that cover both the LTE band 42 and 5.8-GHz WLAN band, the CUAs operate at the LTE band 42. By combining the quasi-orthogonal polarization, balanced mode excitation and pattern diversity, high isolation can be achieved in the operating frequency bands. The proposed antenna array was fabricated and measured. Desirable isolations, envelope correlation coefficients (ECCs), total efficiencies and ergodic channel capacities over the entire operating bands are obtained. The main achievements of this work are as follows: (1) High isolation (more than 17.1 dB) is achieved while supporting the multi-band operation. (2) Cover both the 5G and WLAN bands that are rarely reported but favorable for future multi-network converged system.

II. PROPOSED ANTENNA DESIGN

A. ANTENNA ARRAY GEOMETRY

Fig. 1 shows the geometry and detailed dimensions of proposed antenna array. As depicted in Fig. 1(a), the printed circuit board (PCB) is fabricated using a 0.8-mm thick FR4 substrate ($\varepsilon_r = 4.4$, $\tan\delta = 0.02$) of a length 150 mm

and a width 75 mm. Two FR4 dielectric frames (0.8 mm × 6.2 mm × 75 mm) orthogonally surround the long edges of PCB, making the total dimensions of the antenna array to be 150 mm × 75 mm × 7 mm. In addition, the system ground plane is printed on the back surface of PCB. The proposed 8-antenna array consists of two types of antenna elements, namely the FLAs (Ants 1, 4, 5, 8) and CUAs (Ants 2, 3, 6, 7). The four FLAs are separately loaded near the four corners, and the four CUAs are printed in the middle section of two FR4 dielectric frames.

Figs. 1(b) and (c) illustrate the detailed structure and dimensions of the FLA and CUA. The FLA consists of two branches (namely the left branch and right branch) and a U-shaped ground clearance (UGC). Consider Ant 1 as an example. The left branch is a rectangular metal strip, which is electrically connected to the ground plane by a metallized via-hole (Via-hole 2). The right branch is an L-shaped metal strip, a metallized via-hole (Via-hole 1) is placed at its right end for electrical grounding. The width of both branches and 50-ohm microstrip feedline is 1.5 mm. In the ground plane, two vertical open-end sections of UGC share the same dimension of 1 mm × 1 mm, and the bottom portion of UGC occupies the dimension of 10.6 mm × 1 mm. The FLA is designed to excite dual-band operation that can fully cover the LTE band 42 and 5.8-GHz WLAN band. As for the CUA operating at LTE band 42, it is composed of a rectangular feeding strip (8.2 mm × 1 mm) and a U-shaped metal strip (27.6 mm × 5.6 mm). They are printed at the front and back surface of FR4 dielectric frames, respectively. The U-shaped metal strip is coupled fed by the rectangular feeding strip which is connected directly to a SMA connector.

B. SIMULATED RESULTS AND ANALYSIS

Fig. 2 shows the simulated S parameters of the proposed antenna array in the low band (LB) and high band (HB). The CST Studio Suite 2019 [26] was used to simulate and analyze the proposed antenna array. Owing to the symmetry of this proposed antenna array, for brevity, only the simulated results of Ant 1 to 6 are depicted. As observed in Fig. 2(a), Ants 1 and 2 have sufficient 6-dB impedance matching (across 3:1 Voltage Standing Wave Ratio (VSWR)) over the LTE band 42 (3.4–3.6 GHz), wherein the obtained isolations are greater than 15.5 dB. As shown in Fig. 2(b), Ant 1 exhibits good 10-dB (2:1 VSWR) impedance bandwidths over the 5.8 GHz WLAN band (5.725–5.875 GHz). The isolations between FLAs and CUAs (Ant 1 and Ant 2, Ant 1 and Ant 3) are better than 19.8 dB in the 5.8-GHz WLAN band, indicating the effects of CUAs on FLAs are small. As the FLAs (Ants 1, 4, 5 and 8) work in the 5.8-GHz WLAN band, wherein the CUAs (Ants 2, 3, 6 and 7) do not work. The isolations between FLAs and CUAs are not regarded as the isolations of antenna array in the 5.8-GHz WLAN band. By further observing Fig. 2(b), the isolations between FLAs (Ant 1 and Ant 4, Ant 1 and Ant 5) are higher than 29.0 dB. Therefore, the obtained isolations are greater than 15.5 dB

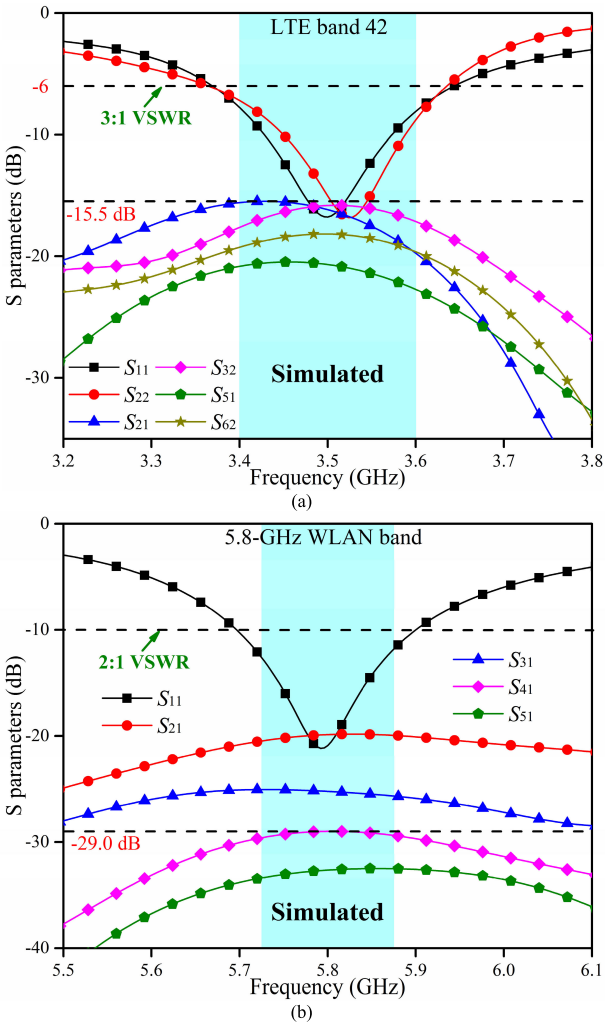

FIGURE 2. Simulated S parameters results of the proposed MIMO antenna array in the (a) LB, (b) HB.

and 29.0 dB in the corresponding frequency bands, which is desirable for MIMO antenna operations.

In order to explain the working modes of FLA, vector current distributions of Ant 1 at two resonant frequencies (3.5 GHz and 5.8 GHz) are shown in Fig. 3. Since the vector current distributions in the upper and back surface of PCB overlap, they are plotted separately. Figs. 3(a) and (b) show that, at 3.5 GHz (the first resonant frequency), the current flows in turn along the path of A → B → C → D → E → F, its intensity reaches the minimum value at point F. The length of above path (A → B → C → D → E → F) is about 17.4 mm ($0.20\lambda_1$, where λ_1 is the wavelength of 3.5 GHz in free space). So, the above path works as the fundamental monopole mode at 3.5 GHz. As observed from Figs. 3(c) and (d), the current at 5.8 GHz (the second resonant frequency) still flows along the original current path (A → B → C → D → E → F). Besides, there is a current null at the point B, the direction of current in the path of A → B inverts as well. That is to say, the path of A → B → C → D → E → F works as the higher-order monopole mode at 5.8 GHz.

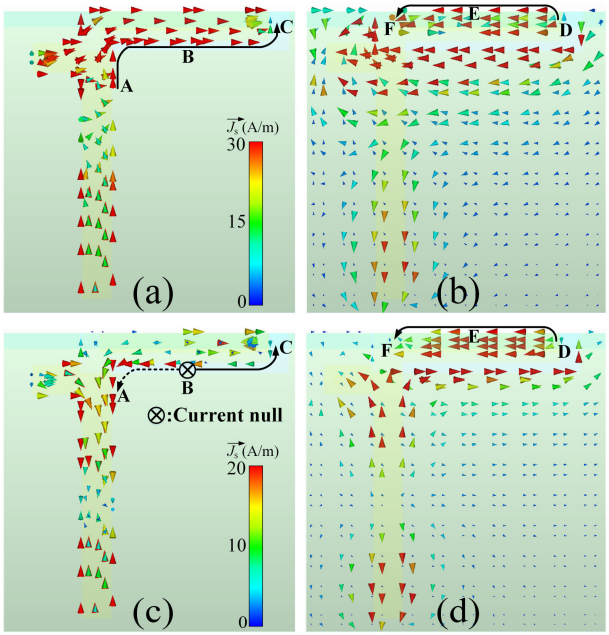

FIGURE 3. Simulated vector current distributions of Ant 1. (a) upper surface of PCB at 3.5 GHz. (b) back surface of PCB at 3.5 GHz. (c) upper surface of PCB at 5.8 GHz. (d) back surface of PCB at 5.8 GHz.

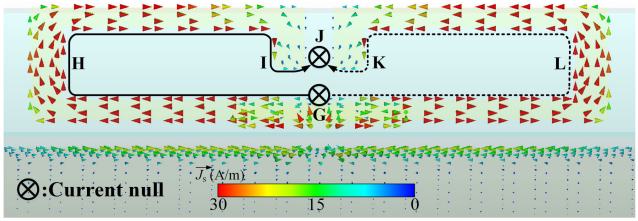

FIGURE 4. Simulated vector current distributions of Ant 2 at 3.5 GHz.

The vector current distributions of CUA at 3.5 GHz are plotted in Fig. 4. The coupled current from rectangular feeding strip flows into the left current path (G → H → I) and right current path (G → L → K), respectively. In addition, the length of these two current paths is about 28.5 mm ($0.33\lambda_1$). At point G, the direction of current inverts and the intensity of current is weak, therefore G is regarded as the current null point. The current path is blocked by the capacitance in the upper section of U-shaped metal strip, which causes a virtual current null in point J. Therefore, the CUA is equivalent to the combination of two half-wavelength dipole antennas (section GHI and GLK) at the two current nulls (points J and G). Besides, the vector current distributions resemble those of 1-wavelength loop mode, therefore the CUA works as a balanced mode at 3.5 GHz. Due to the self-resonance characteristics of the dipole antenna, the intensity of induced ground current is very weak.

III. RESULT AND DISCUSSION

A. PROTOTYPE AND S PARAMETERS

The proposed 8-antenna array was fabricated, and its characteristics (including the S parameters and 2D radiation patterns) were measured and analyzed. The photos of the prototype are shown in Fig. 5, whereas the measured S parameters of the MIMO antenna array are plotted in Fig. 6.

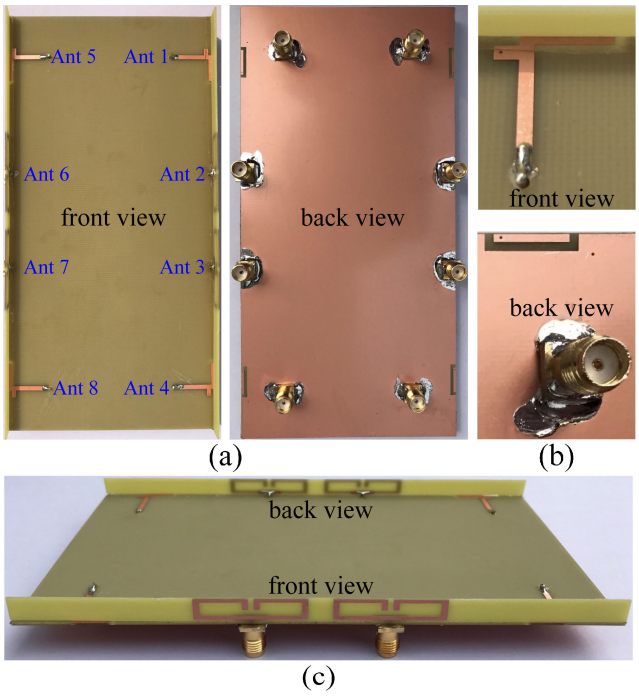

FIGURE 5. Photos of the fabricated 8-antenna array. (a) Overall view of the proposed antenna. (b) Enlarged photo of the FLA. (c) Enlarged photo of the CUA.

Comparing the measured S parameters with the simulated ones in Fig. 2, good agreement is obtained. Some small differences are probably due to the fabrication tolerance and soldering quality of SMA connectors. It is observed in Fig. 6(a) that Ants 1–4 can provide a wide bandwidth (the reflection coefficient lower than –6 dB) to cover the LTE band 42 (3.4–3.6 GHz), wherein the isolations between antenna elements are better than 17.1 dB. As observed in Fig. 6(b), the desirable 5.8 GHz WLAN band (5.725–5.875 GHz) can be fully covered (the reflection coefficient lower than –10 dB) by Ants 1 and 4. The isolation between Ant 1 and Ant 4 is better than 34.6 dB, while that of Ant 1 and Ant 5 is better than 37.4 dB in the operation band. In summary, the measured data indicate that the proposed antenna array can fully cover the LTE band 42 and 5.8 GHz WLAN band with high isolation.

B. RADIATION PERFORMANCE AND MECHANISM OF HIGH ISOLATION

The simulated and measured total efficiencies of the proposed antenna array in the two operation bands are shown in Fig. 7. The method of measuring the total efficiencies is as follows: Theoretically, the total efficiency is the percentage of the total power (measured over the sphere in the far field) to the total input power on the antenna after subtracting the cable loss and path loss in propagation. In our ETS-Lindgren chamber, the antenna under test is used as a transmitter, and the dual polarized horn antenna is used as a receiver. When measuring one antenna element, the other antenna elements

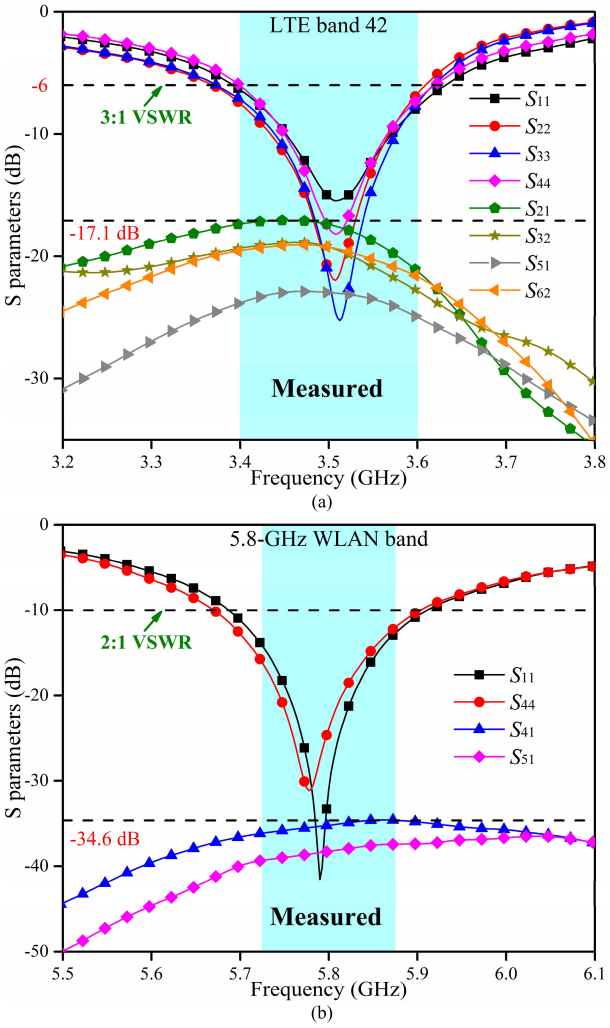

FIGURE 6. Measured S parameters of the proposed MIMO antenna array in the (a) LB, (b) HB.

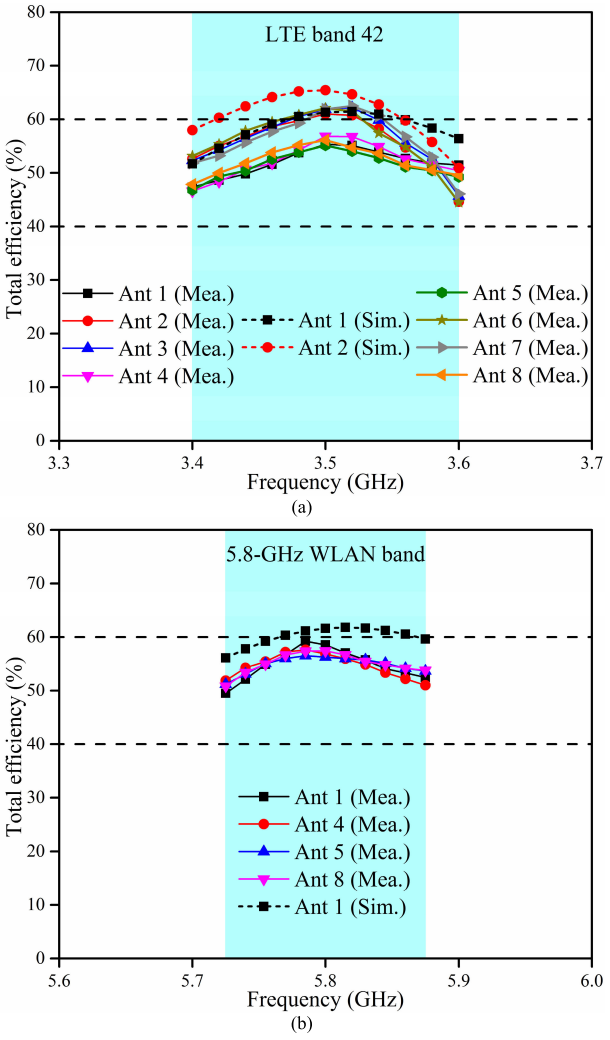

FIGURE 7. Simulated and measured total efficiency in the (a) LTE band 42, (b) 5.8-GHz WLAN band.

are terminated with 50-ohm loads to secure the measurement accuracy. In each total efficiency measurement, the antenna fixture is rotated in two directions of theta and phi (theta = 0–180°, phi = 0–360°) with each step as 5°. In addition, the horn antenna stands still to receive the total power from the vertical and horizontal polarizations. As shown in Fig. 7, the simulated total efficiencies are in good agreement with the measured results. In the LTE band 42, the measured total efficiencies of FLAs (Ants 1, 4, 5, 8) are from 47% to 57%, whereas those of CUAs (Ants 2, 3, 6, 7) range from 45% to 62%. In the 5.8-GHz WLAN band, the measured total efficiencies of FLAs (Ants 1, 4, 5, 8) vary between 52% and 59%. Therefore, the measured total efficiencies of this antenna array are 45%–62% and 52%–59% in the two operation bands, which fulfills the practical requirement (better than 40%) in the smartphones.

In the LTE band 42, the high isolation is achieved by the quasi-orthogonal polarization and balanced mode excitation, while in the 5.8-GHz WLAN band, the high isolation is obtained by the pattern diversity. In order to verify

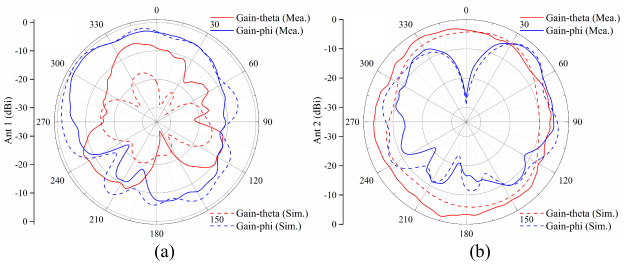

FIGURE 8. Measured and simulated radiation patterns of antennas at xy-plane. (a) Ant 1, 3.5 GHz (b) Ant 2, 3.5 GHz.

the polarization of antenna elements in the LTE band 42, the measured theta-polarized and phi-polarized radiation patterns in the xy plane at 3.5 GHz are shown in Fig. 8. Considering the similarity of measured radiation patterns, the results of Ants 1, 2 are presented. The proposed antenna array has a good agreement between the simulated and measured radiation patterns. As shown in Figs. 8(a) and (b), at 3.5 GHz, Ant 1 shows broadside phi-polarized radiation pattern, while Ant 2 exhibits theta-polarized radiation pattern.

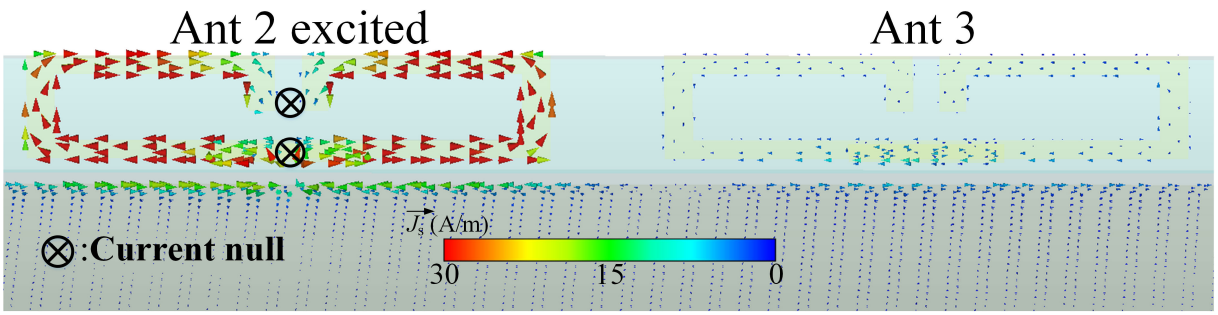

FIGURE 9. Simulated vector current distributions at 3.5 GHz when Ant 2 is excited.

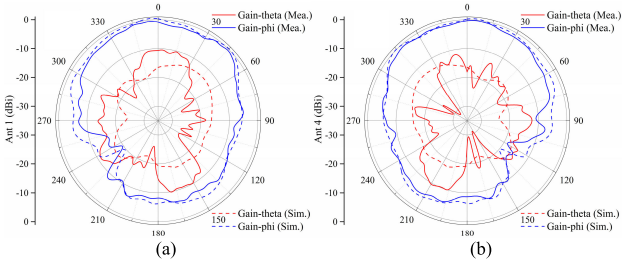

FIGURE 10. Measured and simulated radiation patterns of antennas at xy-plane. (a) Ant 1, 5.8 GHz (b) Ant 4, 5.8 GHz.

The cross-polarization discrimination (XPD) of Ants 1 and 2 are 11.1 dB and 15.3 dB, respectively. Therefore, their quasi-orthogonal polarization characteristic result in the high isolation (Ant 1 and Ant 2) across the LB. The high isolation of opposite antenna elements (such as Ant 2 and Ant 6) is due to the large distance and pattern diversity [27].

To understand mechanism of high isolation between Ant 2 and Ant 3 in the LTE band 42, the vector current distributions at 3.5 GHz for Ants 2 and 3 are presented in Fig. 9. As Ant 2 is excited, the current is almost on Ant 2 rather than the ground plane, therefore the current flowing to Ant 3 is very small. Due to the balanced resonant mode of CUA at 3.5 GHz, good decoupling between Ant 2 and Ant 3 can be obtained.

In order to verify the polarization of antenna elements in the 5.8-GHz WLAN band, the measured theta-polarized and phi-polarized radiation patterns in the xy plane at 5.8 GHz are shown in Fig. 10. As shown in Figs. 10(a) and (b), at 5.8 GHz, Ant 1 and Ant 4 exhibit complementary radiation features in the xy plane, which mainly radiate in the direction of phi = 0°. Since Ant 1 and Ant 4 are far from each other and radiate in the same direction, desirable pattern diversity and good isolation can be obtained in the 5.8-GHz WLAN band.

Hence, in the LTE band 42, the mutual coupling between Ant 1 and Ant 2 is reduced by their quasi-orthogonal polarization characteristics, while the mutual coupling between Ant 2 and Ant 3 is mitigated by the excitation of their balanced resonant modes. In the 5.8-GHz WLAN band, due to the pattern diversity and the large distance separation between two antenna elements (Ant 1 and Ant 4), good isolation can be obtained.

C. MIMO PERFORMANCE

The envelope correlation coefficient (ECC) and ergodic channel capacity are typical functions to evaluate MIMO performance of an antenna array. The ECC describes the correlation between any two antenna elements in a MIMO antenna array. The lower ECC values lead to higher the diversity gain, which are highly expected in the MIMO antenna array [28]. The ECC between antenna i and j can be calculated using the following formula [29]:

$$\rho_{ij} = \frac{\left| \iint_{4\pi} \vec{F}_i(\theta,\varphi) \cdot \vec{F}_j^*(\theta,\varphi) d\Omega \right|^2}{\iint_{4\pi} \left| \vec{F}_i(\theta,\varphi) \right|^2 d\Omega \cdot \iint_{4\pi} \left| \vec{F}_j(\theta,\varphi) \right|^2 d\Omega} \tag{1}$$

where ρ_{ij} denotes the ECC between antenna i and antenna j, $\vec{F}_i(\theta,\varphi)$ and $\vec{F}_j(\theta,\varphi)$ are the field pattern of two radiating elements with respect to θ and φ components, $*$ denotes the complex conjugate operator. Fig. 11 presents the ECC values calculated from the measured complex electric field patterns. In this figure, it is observed that the calculated ECC values are lower than 0.045 and 0.0001 in the LTE band 42 and 5.8-GHz WLAN band, respectively. As smaller ECC values will result in a higher diversity gain, the proposed antenna array has good diversity capability within the operation bands.

In the $N \times N$ MIMO system (N is the number of antennas at the transmitting side), if the transmitter does not know the channel conditions, and the power is equally allocated to every transmitting antenna, the ergodic channel capacity C can be calculated as follows [30]:

$$C = E\left[\log_2 \det\left(\mathbf{I}_N + \frac{SNR}{N} \boldsymbol{H}\boldsymbol{H}^H \right) \right] \tag{2}$$

where E denotes expectation with respect to different channel realizations, $\mathbf{I}_N$ is a $N \times N$ identity matrix, SNR is the mean signal-to-noise ratio at the receiving terminal, $\boldsymbol{H}$ is the $N \times N$ channel matrix, and $(.)^H$ denotes the Hermitian transpose. The calculated ergodic channel capacities of the proposed antenna array for 8×8 MIMO in the LTE band 42 and 4×4 MIMO in the 5.8-GHz WLAN band are presented in Figs. 11(a) and (b). In calculation, it is assumed that the uncorrelated distributed channels obey Rayleigh fading environment and the transmitting antennas are uncorrelated with total efficiencies of 100%. Besides, the ergodic channel capacities of proposed antenna

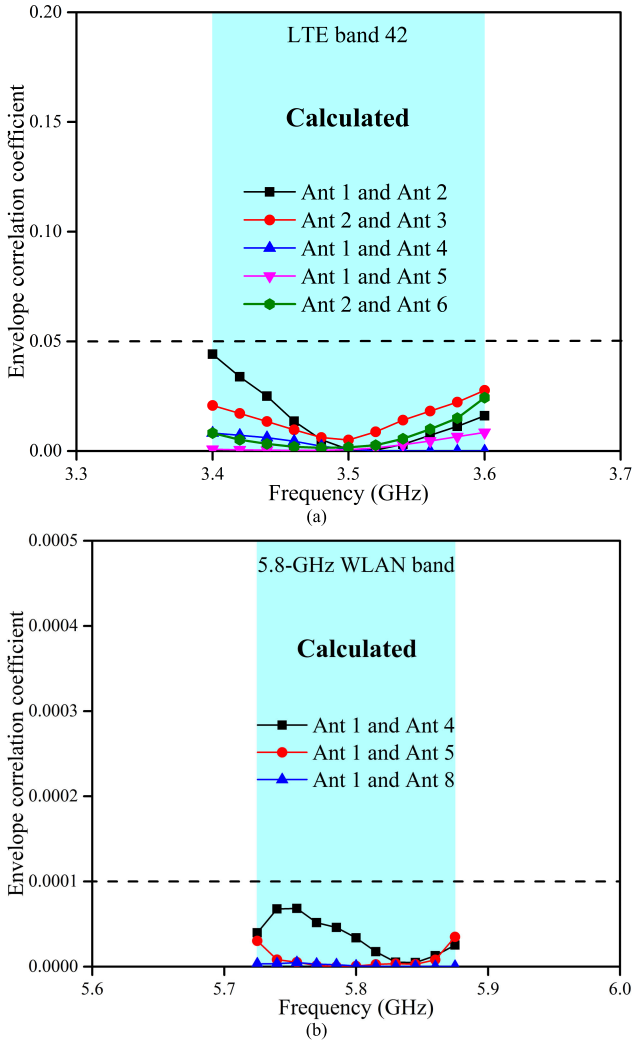

FIGURE 11. Calculated ECC values from the measured data in the (a) LTE band 42, (b) 5.8-GHz WLAN band.

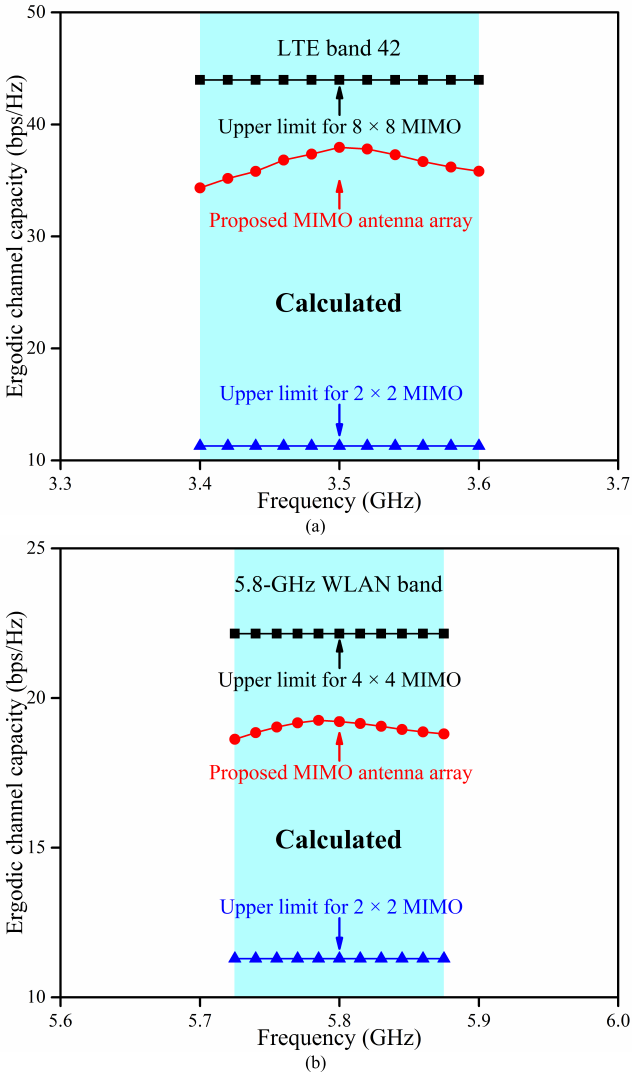

FIGURE 12. Calculated ergodic channel capacity from measured data in the (a) LTE band 42, (b) 5.8-GHz WLAN band.

array are averaged over 100,000 Rayleigh fading realization with the signal-to-noise ratio (SNR) of 20 dB [31]. As shown in Figs. 12(a) and (b), the ergodic channel capacities achieve 34.3–37.9 bps/Hz and 18.6–19.3 bps/Hz for the 8 × 8 MIMO (working in the LTE band 42) and 4 × 4 MIMO (working in the 5.8-GHz WLAN band) system, respectively. The peak ergodic channel capacities (37.9 bps/Hz and 19.3 bps/Hz) in the two operation bands are much better than the upper limit for 2 × 2 MIMO, thereby exhibiting desirable multiplexing capability.

D. USER'S HAND AND HEAD EFFECTS

As human body has a significant impact on antenna performance [32], the effects of user's hand and head are also investigated in this section. The CST Studio Suite 2019 was used to simulate and analyze the user's hand and head effects. Three typical usage scenarios, namely the data mode (DM, single-hand mode), read mode (RM, dual-hands mode) and talk mode (TM, single-hand and head mode), are illustrated in Fig. 13. The simulated S parameters results of the proposed 8-antenna array under the DM, RM and TM are shown in Fig. 14.

For DM condition, the impedance matching of Ants 1, 4 5 and 8 is evidently influenced, especially for Ant 1, as shown in Figs. 14(a) and (b). The reflection coefficients of Ants 2, 3, 6 and 7 are well below –6 dB in the LTE band 42, and those of Ants 4, 5 and 8 are well below –10 dB in the 5.8-GHz WLAN band. While the reflection coefficients of Ant 1 are significantly affected in the two operation bands. In addition, the isolations of antenna array are higher than 14.6 dB and 28.3 dB in the LTE band 42 and 5.8-GHz WLAN band, respectively.

Under RM scenario, because antenna elements on the right hand side (Ants 1, 2, 5 and 6) are symmetric with the antenna elements (Ants 4, 3, 8 and 7) on the left hand side, as shown in Fig. 13(b), only the S parameters of Ants 1, 2, 5, and 6 are illustrated in Figs. 14(c) and (d). It is observed in Fig. 14(c) that Ants 1, 2, 5 and 6 can still provide a sufficient bandwidth

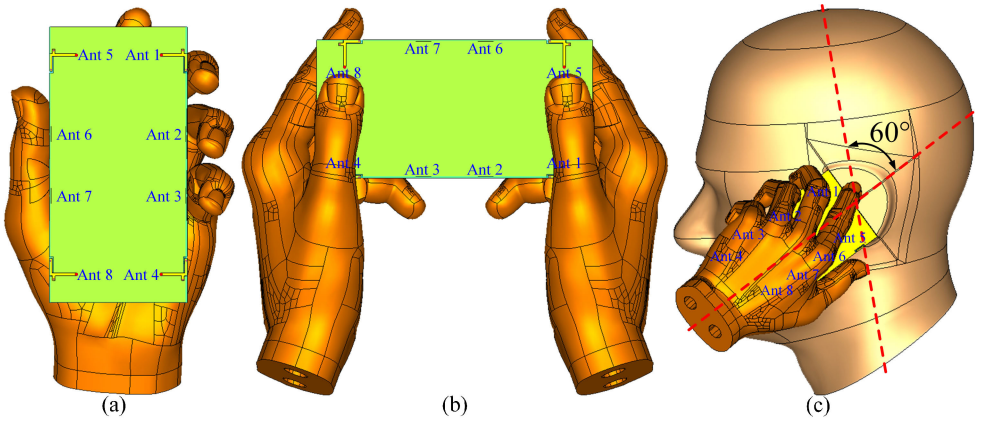

FIGURE 13. Three typical usage scenarios of smartphone. (a) Data mode (DM). (b) Read mode (RM). (c) Talk mode (TM).

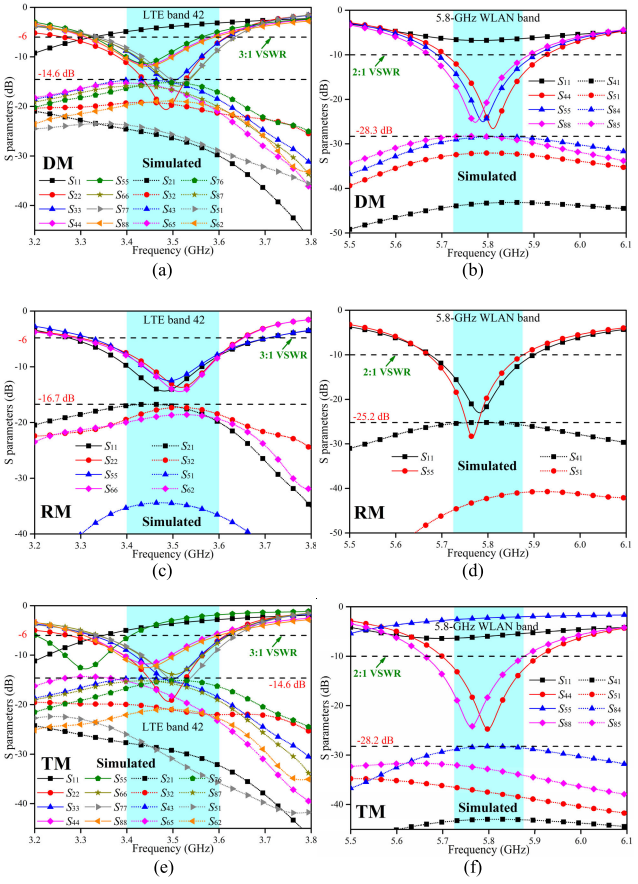

FIGURE 14. Simulated S parameters results with hand and head effects. (a) LB, DM. (b) HB, DM. (c) LB, RM. (d) HB, RM. (e) LB, TM. (f) HB, TM.

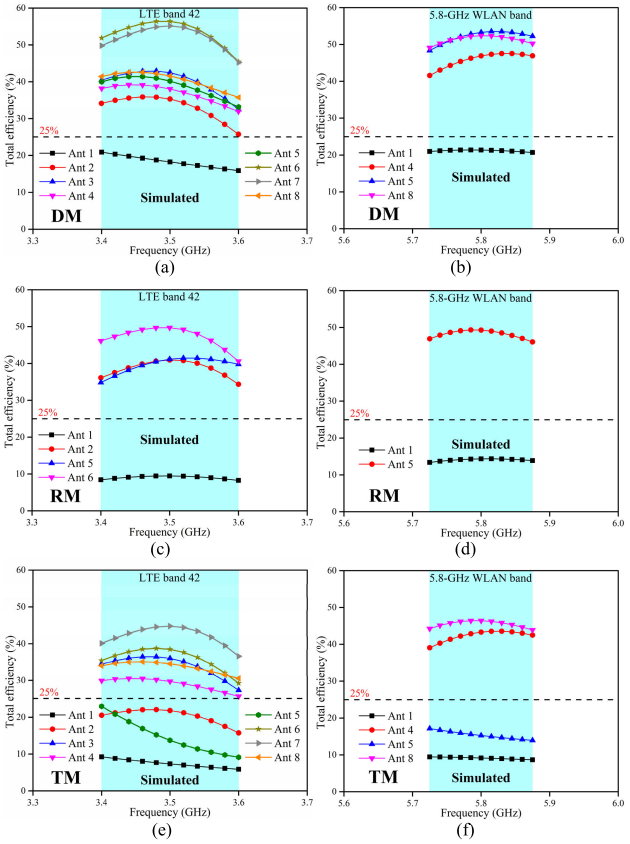

FIGURE 15. Simulated total efficiency results with hand and head effects. (a) LTE band 42, DM. (b) 5.8-GHz WLAN band, DM. (c) LTE band 42, RM. (d) 5.8-GHz WLAN band, RM. (e) LTE band 42, TM. (f) 5.8-GHz WLAN band, TM.

(the reflection coefficient lower than –6 dB) to cover the LTE band 42, wherein the isolations between antenna elements are better than 16.7 dB. As observed in Fig. 14(d), the 5.8 GHz WLAN band can still be supported (the reflection coefficient lower than −10 dB) by Ants 1 and 5, and the high-isolation level (>25.2 dB) can still be maintained.

Under TM scenario, the hand and head phantoms deteriorate the impedance matching of antenna elements, especially for Ants 1 and 5, and the resonant frequencies of Ants 4 and 8 are deviated as shown in Figs. 14(e) and (f). Fortunately, Ants 2, 3, 6, 7 and 8 can still cover the LTE band 42 (–6 dB impedance bandwidth), Ants 4 and 8 can still support the 5.8-GHz WLAN band (–10 dB impedance bandwidth). Besides, the isolations in the two operations bands are higher than 14.6 dB and 28.2 dB, respectively. The above simulated S parameters results certainly indicate that

TABLE 1. A Comparison between the proposed MIMO antenna and other referential works.

Reference	Decoupling method	Isolation (dB)*	Impedance Bandwidth (GHz)	ECC$	Total Efficiency (%)~	Peak channel capacity (bps/Hz)# and number of antennas	Antenna separation (mm^2)@	Antenna size (mm^3)
Proposed	BME, PoD and PaD	> 17.1 (LB) > 34.6 (HB)	LB: 3.4–3.6 (–6 dB) HB: 5.725–5.875 (–10 dB)	< 0.045 (LB) < 0.0001 (HB)	45–62 (LB) 52–59 (HB)	37.9 (LB, 8 × 8) 19.3 (HB, 4 × 4), 8	14.9	32.2 /123.6
[3]	NL	> 10.5 (LB) > 11.0 (HB)	LB: 2.496–2.69 (–6 dB) HB: 3.3–3.7 (–6 dB)	< 0.11 (LB) < 0.06 (HB)	41–54 (LB) 46–64 (HB)	36.9 (LB, 8 × 8) 38.9 (HB, 8 × 8), 8	22.1	570.8
[4]	without	> 12 (LB) > 12.5 (HB)	LB: 3.4–3.8 (–6 dB) HB: 5.15–5.925 (–6 dB)	< 0.15 (LB) < 0.1 (HB)	41–82 (LB) 47–79 (HB)	37 (LB, 8 × 8) 29.5 (HB, 6 × 6), 12	13.8	25.2/14/ 61.6
[5]	PoD and PaD	> 11 (LB) > 11 (HB)	LB: 3.4–3.8 (–6 dB) HB: 5.15–5.925 (–6 dB)	< 0.15 (LB) < 0.2 (HB)	42–65 (LB) 62–82 (HB)	48 (LB, 10 × 10) 51.4 (HB, 10 × 10), 10	23.9	32.4
[7]	PoD and PaD	> 12	3.4–3.8 (–6 dB)	< 0.1	57–78	10.6 (2 × 2), 2	2	29/49.6
[8]	PE	> 15	3.4–3.6 (–10 dB)	NG	34–65	NG, 8	30	33.6
[9]	NL	> 12	3.4–3.6 (–6 dB)	< 0.35	30–52	37 (8 × 8), 8	6	12.8
[11]	PoD and PaD	> 12.5	2.55–2.65 (–10 dB)	< 0.15	48–63	40 (8 × 8), 8	11.3	71.2/ 187.2
[12]	BME, PoD and PaD	> 17.5	3.4–3.6 (–10 dB)	< 0.05	62–76	40.8 (8 × 8), 8	12.8	51.6
[13]	NL and GS	> 15	3.3–3.6 (–6 dB)	< 0.15	45–60	NG, 8	18.5	37.6/49
[14]	OAM and OCM	> 16	3.4–3.6 (–10 dB)	< 0.05	59–73	39.8 (8 × 8), 8	65.6	340.8
[15]	PoD and PE	> 15	3.4–3.8 (–10 dB)	< 0.05	50–75	NG, 8	36.9	276.8
[16]	PE	> 17	3.4–3.6 (–6 dB)	< 0.1	58–75	19 (4 × 4), 4	1.2	52.6
[17]	PE	> 20	3.4–3.6 (–10 dB)	< 0.003	60–67	NG, 8	11.2	138.9
[18]	PE	> 19.1	3.4–3.6 (–10 dB)	< 0.0125	59–68	NG, 8	20.8	83.5
[21]	without	> 11	3.3–3.6 (–10 dB)	< 0.15	50–76	51 (10 × 10), 10	14.7	37.8/54.4
[22]	without	> 11.7	3.4–3.8 (–10 dB)	< 0.1	NG	NG, 8	27.8	52.5
[23]	without	> 10	3.4–3.8 (–6 dB)	< 0.1	40–57	47 (10 × 10), 10	17.5	19.2
[24]	BME	> 13	3.4–3.6 (–6 dB)	< 0.15	42–75	NG, 8	10.8	136.1/36 2.9
[25]^	without	> 10	3.4–3.6 (–10 dB)	< 0.2	62–78	39.7 (8 × 8), 8	17	38.4

Abbreviations: BME=balanced mode excitation, PoD=polarization diversity, PaD=pattern diversity, NL=neutralization line, PE=parasitic element, GS=ground slot, OAM=orthogonal antenna mode, OCM=orthogonal chassis mode, LB=low band, HB=high band, sim.=simulation, mea.=measurement, NG=not given.
* All the isolations are measured data.
$ All the ECC values are measured data, except for [17] (simulated results).
~ All the total efficiencies are measured data, except for [8] and [15] (simulated results).
# All the channel capacities are calculated by assuming SNR = 20 dB.
@ All the Antenna separations are average results.
^ Only 5G antennas are considered.

the proposed 8-antenna array can still work well under the scenario of RM, DM and TM.

On the other hand, how the total efficiency results are influenced by the hand and head phantom are also investigated. Fig. 15 shows the simulated total efficiency results under the effects of hand and head across the two operation bands. As a very lossy medium, hands can absorb a lot of radiated energy of antenna elements [33]. As shown in Fig. 15(a), in the LTE band 42, the total efficiencies of Ant 1 are below 21% under DM scenario, while those of other antenna elements (Ants 2–8) are greater than 25%. This is because Ant 1 is in direct contact with the fingers, others antenna elements are relatively far from the fingers. The absorption losses and resonant frequency deviations of Ant 1 are larger than other antenna elements. As shown in Fig. 15(b), for the DM across the 5.8-GHz WLAN band, the total efficiencies of Ant 1, which is in proximity to the fingers, are below 21%, while Ants 4, 5 and 8 can still work well with desirable total efficiencies (greater than 42%). Therefore, under DM scenario, the proposed 8-antenna array is still good for 7 × 7 (Ants 2–8) and 3 × 3 (Ants 4 5 and 8) MIMO operation across the LTE band 42 and 5.8-GHz WLAN band, respectively.

Under RM scenario, it can be observed that the total efficiencies of Ant 1 are lower than 9% across the LTE band 42, while other antenna elements (Ants 2, 5 and 6) can achieve total efficiencies of 34%–50%, as shown in Fig. 15(c). For the 5.8-GHz WLAN band, the total efficiencies of Ant 1 are

below 14%, whereas Ant 5 can obtain 46%–49% total efficiencies, as shown in Fig. 15(d). Therefore, the proposed 8-antenna array can still work as 6 × 6 (Ants 2, 3, 5, 6, 7 and 8) and 2 × 2 (Ants 5 and 8) MIMO operation in the LTE band 42 and 5.8-GHz WLAN band under the RM condition.

Under TM scenario, the antenna array suffers evident total efficiency degradation. As shown in Fig. 15(e), the total efficiencies of Ants 1, 2 and 5 are reduced to below 23% across the LTE band 42, while the total efficiencies of Ants 3, 4, 6, 7 and 8 are higher than 26%. As shown in Fig. 15(f), in the 5.8-GHz WLAN band, the total efficiencies of Ants 1 and 5 are less than 17%, whereas Ants 4 and 8 demonstrate better total efficiencies of larger than 39%. Hence, the proposed 8-antenna array can work well in 5 × 5 (Ants 3, 4, 6, 7 and 8) and 2 × 2 (Ants 4 and 8) MIMO system across the operation frequency bands under TM condition.

E. PERFORMANCE COMPARSION

A performance comparison among the proposed antenna array and previously reported works is summarized in Table 1. The proposed 8-antenna array adopts three intrinsic decoupling methods, which incurs no additional efficiency loss and easy to be implemented. Compared with multi-band antenna arrays, the proposed antenna array achieves higher isolations. Compared with those of high-isolation antenna arrays that cover single frequency band, the proposed antenna array supports multi-band operation. Moreover, the proposed antenna array has a simple structure and low ECC values. Its total efficiency, peak channel capacity and antenna separation are also comparable to those of other antenna arrays. Lastly, the proposed antenna array converges the 5G and WLAN bands for future multi-network converged system.

IV. CONCLUSION

In this article, a dual-functional MIMO antenna array for 5G/WLAN applications in smartphones is proposed. By integrating eight antenna elements (of two types, namely, FLA and CUA), the proposed antenna array can be applied in the 8 × 8 and 4 × 4 MIMO system across the LTE band 42 and 5.8-GHz WLAN band. High isolation can also be achieved by applying the quasi-orthogonal polarization, balanced mode excitation and pattern diversity techniques. Additionally, it achieves good isolations of better than 17.1 dB, desirable ECCs of lower than 0.045, and high total efficiencies of more than 45% within the operation bands. The calculated ergodic channel capacities for the 8 × 8 MIMO (working in the LTE band 42) and 4 × 4 MIMO (working in the 5.8-GHz WLAN band) are 34.3–37.9 bps/Hz and 18.6–19.3 bps/Hz, respectively. Besides, the proposed antenna has advantages of small ground clearance and simple structure. Due to the above good performance, this proposed antenna array could be a promising choice for 5G/WLAN applications in smartphones.

REFERENCES

[1] W. Hong, "Solving the 5G mobile antenna puzzle: Assessing future directions for the 5G mobile antenna paradigm shift," *IEEE Microw. Mag.*, vol. 18, no. 7, pp. 86–102, Nov. 2017.

[2] H. Zou, Y. Li, C.-Y.-D. Sim, and G. Yang, "Design of 8 × 8 dual-band MIMO antenna array for 5G smartphone applications," *Int. J. RF Microw. Comput. Aided Eng.*, vol. 28, no. 9, Nov. 2018, Art. no. e21420.

[3] H. Zou, Y. Li, B. Xu, Y. Luo, M. Wang, and G. Yang, "A dual-band eight-antenna multi-input multi-output array for 5G metal-framed smartphones," *Int. J. RF Microw. Comput. Aided Eng.*, vol. 29, no. 7, Jul. 2019, Art. no. e21745.

[4] Y. Li, C.-Y.-D. Sim, Y. Luo, and G. Yang, "12-port 5G massive MIMO antenna array in sub-6GHz mobile handset for LTE bands 42/43/46 applications," *IEEE Access*, vol. 6, pp. 344–354, Oct. 2017.

[5] Y. Li, C.-Y.-D. Sim, Y. Luo, and G. Yang, "Multiband 10-antenna array for sub-6 GHz MIMO applications in 5-G smartphones," *IEEE Access*, vol. 6, pp. 28041–28053, May 2018.

[6] J. Li, X. Zhang, Z. Wang, X. Chen, J. Chen, Y. Li, and A. Zhang, "Dual-band eight-antenna array design for MIMO applications in 5G mobile terminals," *IEEE Access*, vol. 7, pp. 71636–71644, 2019.

[7] K.-L. Wong and H.-J. Chang, "Hybrid dual-antenna for the 3.6-GHz LTE operation in the tablet computer," *Microw. Opt. Technol. Lett.*, vol. 57, pp. 2592–2598, Nov. 2015.

[8] H. Xu, H. Zhou, S. Gao, H. Wang, and Y. Cheng, "Multimode decoupling technique with independent tuning characteristic for mobile terminals," *IEEE Trans. Antennas Propag.*, vol. 65, no. 12, pp. 6739–6751, Dec. 2017.

[9] K. L. Wong, J.-Y. Lu, L.-Y. Chen, W.-Y. Li, and Y.-L. Ban, "8-antenna and 16-antenna arrays using the quad-antenna linear array as a building block for the 3.5-GHz LTE MIMO operation in the smartphone," *Microw. Opt. Technol. Lett.*, vol. 58, no. 1, pp. 174–181, Jan. 2016.

[10] R. Saleem, M. Bilal, K. B. Bajwa, and M. F. Shafique, "Eight-element UWB-MIMO array with three distinct isolation mechanisms," *Electron. Lett.*, vol. 51, no. 4, pp. 311–313, Feb. 2015.

[11] M.-Y. Li, Y.-L. Ban, Z.-Q. Xu, G. Wu, C.-Y.-D. Sim, K. Kang, and Z.-F. Yu, "Eight-port orthogonally dual-polarized antenna array for 5G smartphone applications," *IEEE Trans. Antennas Propag.*, vol. 64, no. 9, pp. 3820–3830, Sep. 2016.

[12] Y. Li, C.-Y.-D. Sim, Y. Luo, and G. Yang, "High-isolation 3.5 GHz eight-antenna MIMO array using balanced open-slot antenna element for 5G smartphones," *IEEE Trans. Antennas Propag.*, vol. 67, no. 6, pp. 3820–3830, Jun. 2019.

[13] W. Jiang, B. Liu, Y. Cui, and W. Hu, "High-isolation eight-element MIMO array for 5G smartphone applications," *IEEE Access*, vol. 7, pp. 34104–34112, 2019.

[14] A. Ren, Y. Liu, and C.-Y.-D. Sim, "A compact building block with two shared-aperture antennas for eight-antenna MIMO array in metal-rimmed smartphone," *IEEE Trans. Antennas Propag.*, vol. 67, no. 10, pp. 6430–6438, Oct. 2019, doi: 10.1109/TAP.2019.2920306.

[15] N. O. Parchin, Y. I. A. Al-Yasir, A. H. Ali, I. Elfergani, J. M. Noras, J. Rodriguez, and R. A. Abd-Alhameed, "Eight-element dual-polarized MIMO slot antenna system for 5G smartphone applications," *IEEE Access*, vol. 7, pp. 15612–15622, 2019.

[16] Z. Ren, A. Zhao, and S. Wu, "MIMO antenna with compact decoupled antenna pairs for 5G Mobile terminals," *IEEE Trans. Antennas Propag. Lett.*, vol. 18, no. 7, pp. 1367–1371, Jul. 2019, doi: 10.1109/LAWP.2019.2916738.

[17] A. Zhao and Z. Ren, "Multiple-input and multiple-output antenna system with self-isolated antenna element for fifth-generation mobile terminals," *Microw. Opt. Technol. Lett.*, vol. 61, pp. 20–27, Jan. 2019.

[18] A. Zhao and Z. Ren, "Size reduction of self-isolated MIMO antenna system for 5G mobile phone applications," *IEEE Antennas Wireless Propag. Lett.*, vol. 18, no. 1, pp. 152–156, Jan. 2019.

[19] S. Xu, Y. Li, Y. Gao, Y. Liu, and H. Gačanin, "Opportunistic coexistence of LTE and WiFi for future 5G system: Experimental performance evaluation and analysis," *IEEE Access*, vol. 6, pp. 8725–8741, 2018.

[20] Qualcomm. *What Can We Do With 5G NR Spectrum That Isn't Possible Today?* Accessed: Dec. 13, 2017. [Online]. Available: https://www.qualcomm.com/media/documents/files/new-3gpp-effort-on-nr-in-unlicensed-spectrum-expands-5g-to-new-areas.pdf

[21] J.-Y. Deng, J. Yao, D.-Q. Sun, and L.-X. Guo, "Ten-element MIMO antenna for 5G terminals," *Microw. Opt. Technol. Lett.*, vol. 60, no. 12, pp. 3045–3049, Dec. 2018.

[22] H. Shi, X. Zhang, J. Li, P. Jia, J. Chen, and A. Zhang, "3.6-GHz eight-antenna MIMO array for mobile terminal applications," *AEU Int. J. Electron. Commun.*, vol. 95, pp. 342–348, Oct. 2018.
[23] K.-L. Wong and J. Y. Lu, "3.6-GHz 10-antenna array for mimo operation in the smartphone," *Microw. Opt. Technol. Lett.*, vol. 57, no. 7, pp. 1699–1704, Jul. 2015.
[24] D. Huang, Z. Du, and Y. Wang, "Slot antenna array for fifth generation metal frame mobile phone applications," *Int. J. RF Microw. Comput. Aided Eng.*, vol. 29, no. 9, 2019, Art. no. e21841, doi: 10.1002/mmce.21841.
[25] Y.-L. Ban, C. Li, C.-Y.-D. Sim, G. Wu, and K.-L. Wong, "4G/5G multiple antennas for future multi-mode smartphone applications," *IEEE Access*, vol. 4, pp. 2981–2988, 2016.
[26] *Computer Simulation Technology (CST) Microwave Studio Suite 2019*. Accessed: Mar. 14, 2019. [Online]. Available: http://www.cst.com
[27] C. F. Ding, X. Y. Zhang, C.-D. Xue, and C.-Y.-D. Sim, "Novel pattern-diversity-based decoupling method and its application to multielement MIMO antenna," *IEEE Trans. Antennas Propag.*, vol. 66, no. 10, pp. 4976–4985, Oct. 2018.
[28] S. Chouhan, D. K. Panda, M. Gupta, and S. Singhal, "Multiport MIMO antennas with mutual coupling reduction techniques for modern wireless transreceive operations: A review," *Int. J. RF Microw. Comput. Aided Eng.*, vol. 28, no. 2, Feb. 2018, Art. no. e21189.
[29] H. Li, X. Lin, B. K. Lau, and S. He, "Equivalent circuit based calculation of signal correlation in lossy MIMO antennas," *IEEE Trans. Antennas Propag.*, vol. 61, no. 10, pp. 5214–5222, Oct. 2013.
[30] A. A. Al-Hadi, J. Ilvonen, R. Valkonen, and V. Viikari, "Eight-element antenna array for diversity and mimo mobile terminal in LTE 3500 MHz band," *Microw. Opt. Technol. Lett.*, vol. 56, no. 6, pp. 1323–1327, Jun. 2014.
[31] R. Tian, B. K. Lau, and Z. Ying, "Multiplexing efficiency of MIMO antennas," *IEEE Antennas Wireless Propag. Lett.*, vol. 10, pp. 183–186, 2011.
[32] B. Xu, Y. Li, and Y. Kim, "Classification of finger movements based on reflection coefficient variations of a body-worn electrically small antenna," *IEEE Antennas Wireless Propag. Lett.*, vol. 16, pp. 1812–1815, 2017.
[33] K. Zhao, S. Zhang, K. Ishimiya, Z. Ying, and S. He, "Body-insensitive multimode MIMO terminal antenna of double-ring structure," *IEEE Trans. Antennas Propag.*, vol. 63, no. 5, pp. 1925–1936, May 2015.

HUANQING ZOU was born in Zhejiang, China, in 1990. He is currently pursuing the Ph.D. degree in electromagnetic field and microwave technology with Shanghai University, China. His current research interests include MIMO antenna arrays, 5G smartphone antennas, multiband antennas, and millimeter-wave antennas. He is serving as a Reviewer for IEEE Access and the *International Journal of RF and Microwave Computer-Aided Engineering*.

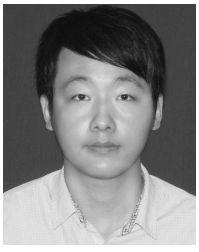

YIXIN LI was born in Hunan, China, in 1994. He received the B.S. and M.S. degrees from Shanghai University, Shanghai, China, in 2016 and 2019, respectively. He is currently pursuing the Ph.D. degree in electromagnetic field and microwave technology with the School of Electronic and Information Engineering, South China University of Technology, Guangzhou, China. His current research interests include electrically small antennas, mobile terminal antennas, MIMO antennas, 5G antennas, and antenna decoupling. He is currently serving as a Reviewer for IEEE Access, *AEÜ-International Journal of Electronics and Communications*, and the *Applied Computational Electromagnetics Society* (ACES) Journal.

BIN XU received the B.S. and M.S. degrees in electrical engineering from Xidian University, Xi'an, China, in 2010 and 2013, respectively, and the Ph.D. degree from Baylor University, in 2018. He joined Qualcomm as a Senior RF Engineer, responsible for state-of-art front end circuit design. His current research interests include electrically antennas, wearable antennas, 5G/sub-6 MIMO antenna arrays, and RF front end circuits.

YUANQING CHEN (S'19) received the B.S. degree from Shanghai University, China, in 2018, where he is currently pursuing the M.S. degree in electromagnetic field and microwave technology. Since 2018, he has been with the Institute for Advanced Communication and Data Science, Shanghai University. His current research interests include millimeter-wave communication, massive MIMO/MIMO systems, system design, and signal processing for millimeter-wave radar.

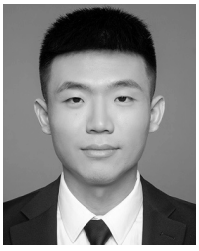

HAO JIN was born in Shanxi, China, in 1995. He received the B.S. degree in electronic science and technology from the Shanghai University of Electric Power, Shanghai, China, in 2017. He is currently pursuing the M.S. degree in electromagnetic fields and microwave technology with the School of Communication and Information Engineering, Shanghai University, Shanghai, China. His current research interests include dual-polarized antenna array, cost-effective RF phase shifting module, and communication receiver.

GUANGLI YANG (M'06) received the B.S. degree in physics from the Beijing University of Science and Technology, Beijing, China, in 1997, and the Ph.D. degree in electrical engineering from the University of South Carolina, Columbia, SC, USA, in 2005. From 2005 to 2013, he was with the Antenna and RF Research Group, Motorola Inc., Chicago, IL, USA, where he started as Senior Staff and was then promoted Principal Engineer. Since 2014, he has been a Professor with Shanghai University, Shanghai, China, where he is currently the Director of the RF Research Group. He has authored or coauthored more than 60 publications. He holds 21 patents filed or issued. His current research interests include smart antennas, antenna miniaturization and configurability, digital beamforming system, and microwave circuits. He was a recipient of the Shanghai Eastern Scholarship Awards in 2013.

YONG LUO received the Ph.D. degree from The University of Tokyo, Tokyo, Japan, in 2015, with a focus on active metamaterials for scanning radiation beams by using micromachining fabrication process to monolithically integrate antenna with MEMS. From 2010 to 2012, he was an Electrical Engineer with Huawei, Shanghai, China, where he involved in phased array antennas for base stations. He was with Prof. Sievenpiper's Applied Electromagnetic Group, San Diego, CA, USA, where he held a Postdoctoral position in nonlinear metasurfaces using diodes in 2016. He is currently an Assistant Professor with the Department of Electronic and Information Engineering, School of Communication and Information Engineering, Shanghai University, Shanghai. His current research interests include active antennas, nonlinear metamaterial, and RF-MEMS.